Battery-free 802.15.4 Receiver

Carlos Pérez-Penichet
Uppsala University
Sweden
carlos.penichet@it.uu.se

Claro Noda
Mid-Sweden University
Sweden
claro.noda@miun.se

Ambuj Varshney
Uppsala University
Sweden
ambuj.varshney@it.uu.se

Thiemo Voigt
Uppsala University and RISE SICS
Sweden
thiemo@sics.se

ABSTRACT

We present the architecture of an 802.15.4 receiver that, for the first time, operates at a few hundred microwatts, enabling new battery-free applications. To reach the required micro-power consumption, the architecture diverges from that of commodity receivers in two important ways. *First*, it offloads the power-hungry local oscillator to an external device, much like backscatter transmitters do. *Second*, we avoid the energy cost of demodulating a phase-modulated signal by treating 802.15.4 as a frequency-modulated one, which allows us to receive with a simple passive detector and an energy-efficient thresholding circuit. We describe a prototype that can receive 802.15.4 frames with a power consumption of 361 µW. Our receiver prototype achieves sufficient communication range to integrate with deployed wireless sensor networks (WSNs). We illustrate this integration by pairing the prototype with an 802.15.4 backscatter transmitter and integrating it with unmodified 802.15.4 sensor nodes running the TSCH and Glossy protocols.

ACM Reference format:
Carlos Pérez-Penichet, Claro Noda, Ambuj Varshney, and Thiemo Voigt. 2018. Battery-free 802.15.4 Receiver. In *Proceedings of International Conference on Information Processing in Sensor Networks, Porto, Portugal, April 2018 (IPSN'18),* 12 pages.
DOI: 10.475/123_4

1 INTRODUCTION

Battery-free sensors are an attractive complement to traditional sensor nodes. The low cost, ease of deployment and low maintenance demands that result from an endless supply of harvested energy from the environment enable novel applications such as implanted devices [17], wearable sensors [37] and smart cities [34]. Rapid progress is being made in several fronts to make practical battery-free sensors a reality. Energy harvesting technologies improve their efficiency at a fast pace, while new harvesting modalities continue to appear [7]. The energy efficiency of digital processing and storage technologies continues to improve, while some works entirely sidestep these functions [31, 36]. Communication has traditionally been a major concern in these scenarios, but new backscatter techniques enable transmissions compatible with standard wireless protocols such as BLE, WiFi and 802.15.4 that consume mere microwatts [12, 17, 20, 27]. These transmissions create the possibility of integrating battery-free devices that harvest minute amounts of energy from previously unusable sources into existing sensor networks. The last remaining obstacle for this integration is the lack of devices that receive standard wireless transmissions with micropower consumption.

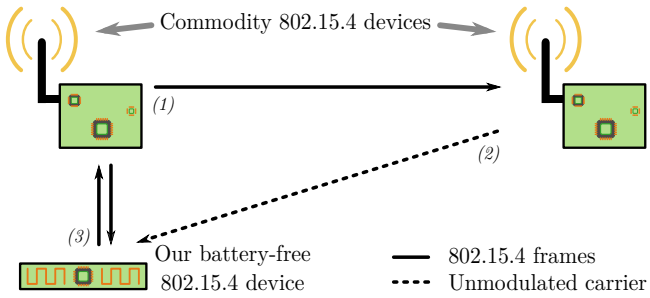

Figure 1: *Our receiver seamlessly integrates with unmodified commodity 802.15.4 devices.* The interrogating node requests a carrier from a neighboring node (1) The carrier (2) is used by our battery-free device to transmit and receive 802.15.4 frames (3) without modifications to the commodity devices.

Contribution. We present an 802.15.4 receiver that, for the first time, operates at a few hundred microwatts. This receiver, paired with a compatible backscatter transmitter [17, 27], enables battery-free devices to transmit and receive 802.15.4 frames assisted by an unmodulated carrier. Such a device can integrate into existing wireless sensor networks without modifications to the deployed infrastructure (Figure 1). A two-way link between the battery-free device and standard 802.15.4 nodes enables the former to implement essential functions such as receiving queries and acknowledgements, time synchronization and medium access coordination.

To illustrate this possibility, we integrate our prototype with unmodified commodity sensor nodes running the Time-Slotted Channel Hopping (TSCH) link-layer protocol [16]. The nodes then coordinate to provide the unmodulated carrier and interrogate the tag for a sensor reading as depicted in Figure 1. We also show

IPSN'18, Porto, Portugal

DOI: 10.475/123_4

how the Glossy protocol [14] could be used to flood information to multiple tags deployed in a network.

In summary, we make the following novel contributions:

- We introduce a receiver that interoperates with 802.15.4 transceivers while consuming two orders of magnitude less power than commercial low-power alternatives, making it compatible with battery-free operation.
- Our receiver prototype achieves sufficient communication range to integrate with common wireless sensor network platforms, utilizing existing nodes as both transmitters and carrier generators.
- The receiver significantly lowers the bar for the integration of battery-free devices into 802.15.4 networks, which we illustrate by integrating it into TSCH- and Glossy-based 802.15.4 networks.

Challenges. Current battery-free devices use passive envelope detectors for reception. Envelope detectors are efficient and enable the reception of amplitude-modulated signals, but are incompatible with standard wireless protocols like BLE, WiFi and 802.15.4 that do not use amplitude modulation. Proposed solutions resort to a variety of mechanisms to sidestep the lack of a compatible receiver. Some works propose an external device that acts as an interpreter between the standard devices and the battery-free ones [19, 20, 35]. Others employ modified Wi-Fi devices that mimic amplitude-modulated signals [17, 19]. Both solutions hinder the seamless integration of battery-free devices into existing networks because they increase the cost and complexity of deployment by requiring added elements or mechanisms.

Conventional 802.15.4 receivers employ power-hungry high-frequency analog and digital blocks such as the Radio Frequency (RF) Low-Noise Amplifier (LNA), RF Local Oscillator (LO) and Analog-to-Digital Converter (ADC). As a consequence, the excellent performance of those receivers comes at the expense of a power consumption in the order of milliwatts, making them inappropriate for battery-free devices.

Approach. To achieve ultra-low-power operation, we sidestep those power-hungry blocks by employing passive circuits whenever possible. We leverage on the proof-of-concept receiver architecture that Ensworth et al. [11] introduced to receive BLE, which uses Frequency Shift Keying (FSK). We borrow their principle of the external oscillator to offload the LO to an external device that broadcasts an unmodulated carrier but apply it to the reception of 802.15.4, which uses Offset-Quadrature Phase Shift Keying (O-QPSK) modulation. Our key insight is that we apply a technique that allows us to treat the phase-modulated 802.15.4 signal as a frequency-modulated one. As a consequence we are able to efficiently demodulate the 802.15.4 signal. Unlike Ensworth et al. [11], we employ a passive frequency detector to further reduce the power consumption and introduce bias in the mixer to regain sensitivity. Furthermore, we build fully working prototypes and integrate them with unmodified commodity 802.15.4 radios. We also provide results on the power consumption of an equivalent integrated receiver implementation.

Using off-the-shelf components, we build two different, fully working prototypes that we employ in our performance evaluation. The first version has no Intermediate Frequency (IF) amplification and the second has additional IF gain and better performance at the expense of the additional power invested in the amplifier. Due to the use of off-the-shelf components for the IF amplifier and an FPGA development board for the Digital Baseband Processor (DBP), these prototypes do not operate at microwatts. To evaluate the power consumption of our receiver, we design an Integrated Circuit (IC) version with a custom IF amplifier and DBP using a generic 45 nm bulk Complementary Metal-Oxide-Semiconductor (CMOS) process.

Results. Our off-the-shelf prototype achieves a communication range of 75 cm without IF amplification and with the carrier generator 40 cm from the receiver, while using a transmitter and carrier output powers of 20 dBm and 25 dBm. When an IF amplifier is added, the range is extended significantly and the signal output power requirements are reduced. The IC implementation, with comparable IF gain, consumes 361 µW.

The receiver seamlessly integrates with commodity 802.15.4 nodes running the TSCH protocol. In this context it exhibits a reliability above 99%. It missed a small number of interrogations over more than 500 000 cycles in an office environment.

Outline. We continue the paper by discussing how our work differs from others in Section 2. We present the design of our architecture, along with some necessary background, in Section 3; while the hardware implementation is discussed in Section 4. Section 5 contains the evaluation of our receiver, and in Section 6 we illustrate the possibility of integrating battery-free devices into standard 802.15.4 networks. In Section 7 we discuss further aspects of this work and in Section 8 we present our conclusions.

2 RELATED WORK

Our work is related to backscatter communications because, like backscatter transmitters, it relies on an externally generated carrier to achieve micropower operation. Likewise, works focused on the design of low-power receivers are related to our work. In this section, we give an overview of how our contribution differs from the related work.

2.1 Low-Power Receivers

Ensworth et al. [11] propose a 2.4 GHz receiver front-end with a two-port mixer and external LO intended for BLE reception. They demonstrate the principle with a benchtop proof-of-concept experiment using mains powered components and capture the baseband to a computer to decode it off-line. The focus of their work is on receiving BLE signals, which use FSK. They do not provide any power consumption information. In this work we use the principle of the external oscillator to receive 802.15.4 signals, which use O-QPSK modulation. Our main contribution is the ability to receive phase modulated signals without the need for power-hungry carrier synchronization. Further, we build a working prototype designed for minimum power consumption. We deviate from their design in that we employ a passive frequency detector and add bias to the diode mixer. We show that an equivalent IC implementation would consume just a few hundred microwatts. Further, we demonstrate that the prototype interoperates with commodity 802.15.4 radios.

We compare our prototype with works focused on reducing the power consumption of radio receivers. Liu et al. [23] present a receiver that consumes 3.8 mW. Khan and Wentzloff [21] introduce a short-range communication receiver for IEEE 802.15.4 that

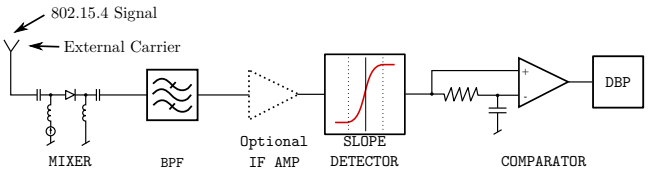

Figure 2: *Our micro-power 802.15.4 receiver architecture.* We avoid power-hungry components and use an external carrier to receive 802.15.4 transmissions consuming microwatts.

consumes only 2.0 mW. Our experiments show that our prototype consumes at least five times less power and has a similar sensitivity as their receiver.

A direct conversion BLE receiver front-end proposed by Bryant and Sjöland [8] has a power consumption of 550 µW with a sensitivity of −70 dBm. However, this power consumption is for a 65 nm CMOS implementation that includes neither a demodulator nor a digital baseband processor. Our architecture is a complete design and it would consume significantly less power if it was implemented with a similar CMOS process.

2.2 Backscatter Communication

Our receiver, when paired with an 802.15.4 backscatter transmitter, enables the seamless integration of battery-free devices into standard wireless sensor networks.

Many recent efforts focus on creating battery-free devices capable of interoperating with commodity wireless devices. They adopt different strategies to receive data at the battery-free device using only Amplitude Shift Keying (ASK) receivers. Some works [17, 19] use customized WiFi devices to create amplitude variations in the WiFi signal that are decoded at the battery-free device using an envelope detector. Such solutions suffer from a high cost of deployment as they require customized WiFi radios.

Other works [12, 17, 20, 27, 30, 35] can transmit commodity wireless protocols using backscatter communications but, for reception, use envelope detectors incompatible with those protocols. For instance, Passive WiFi [20] utilizes a mains-powered device to act as an interpreter between commodity WiFi devices and the battery-free ones that can only receive amplitude-modulated signals.

Both approaches hinder the integration of these solutions with standard wireless networks because of their need for additional devices or mechanisms. Our work eliminates the need for such solutions by enabling micro-powered devices to interoperate with existing 802.15.4-based sensor nodes with no additional infrastructure or hardware modification.

To implement the 802.15.4 transmitter in our prototype, we employ the contributions of our previous work [27] and those of Iyer et al. [17] that feature backscattered 802.15.4 transmissions.

3 ULTRA-LOW-POWER DESIGN

To achieve ultra-low-power operation, we sidestep many of the power-hungry blocks used in 802.15.4 receivers by employing passive circuits whenever possible. We leverage the BLE receiver architecture introduced by Ensworth et al. [11] to offload the power-hungry LO to an external device. Likewise, we avoid power-hungry

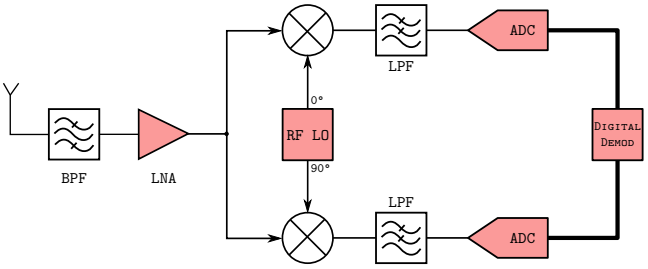

Figure 3: *Simplified architecture of a typical 802.15.4 receiver.* This architecture relies on power-hungry blocks (solid color) such as the LNA, LO, ADCs and the digital demodulator.

multi-bit ADCs and digital demodulators by demodulating in the analog domain. Finally, our crucial insight is our way of efficiently demodulating the 802.15.4 phase-modulated signal by treating it as a frequency modulated one.

In this section, we summarize the modulation scheme defined in the 802.15.4 standard. We then describe how our receiver overcomes the various challenges to receive 802.15.4 frames with ultra-low power consumption.

3.1 The 802.15.4 Standard

The IEEE 802.15.4 Standard [16] defines all aspects of the physical-layer along with some of the link layer. The standard mandates a Direct Sequence Spread Spectrum (DSSS) mechanism to increase robustness. Transmitted data is grouped into symbols that correspond to one of 16 possible 32-chip quasi-orthogonal pseudo-random spreading sequences. These chip sequences are transmitted using O-QPSK with half-sine pulse shaping at a rate ($1/T_c$) of two million chips per second.

O-QPSK encodes the data into four carrier phase offsets. To reduce undesired amplitude fluctuations in the signal, there is a time offset $T_c = 0.5\,\mu s$ between the in-phase (I) and quadrature (Q) components. To further reduce the amplitude fluctuations, 802.15.4 uses half-sine pulse shaping.

The modulated O-QPSK signal $S(t)$ has the form

$$S(t) = a_I(t)\cos\left(\frac{\pi t}{2T_c}\right)\cos(2\pi f t) - a_Q(t)\sin\left(\frac{\pi t}{2T_c}\right)\sin(2\pi f t) \quad (1)$$

where $a_I(t)$ and $a_Q(t)$ represent the data streams to be transmitted (1 for a data 1 and −1 for a data 0) in the I and Q components respectively and f is the frequency of the carrier. The four possible combinations of values of a_I and a_Q correspond to the four different phases of the modulated signal.

To recover the data, a receiver must perform the process in the reverse order, O-QPSK demodulation and then DSSS despreading.

3.2 Ultra-Low-Power 802.15.4 Reception

Receiving 802.15.4 frames while consuming microwatts is challenging due to three main reasons. First, the RF blocks such as LNAs and LO used to condition the signal are power hungry. Second, demodulating in the digital domain is power hungry due to the ADCs and

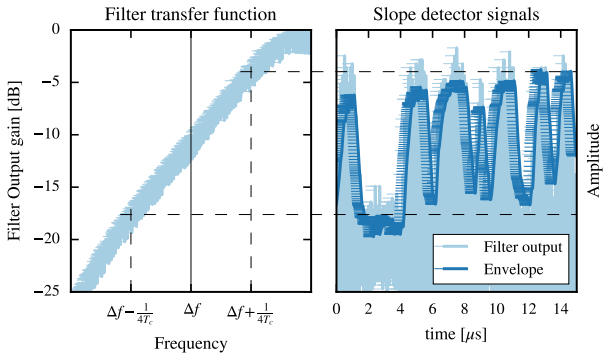

Figure 4: *The operation of the slope detector.* The frequency variations of the signal are translated into amplitude variations. The final output of the slope detector (highlighted on the right) results from an envelope detector.

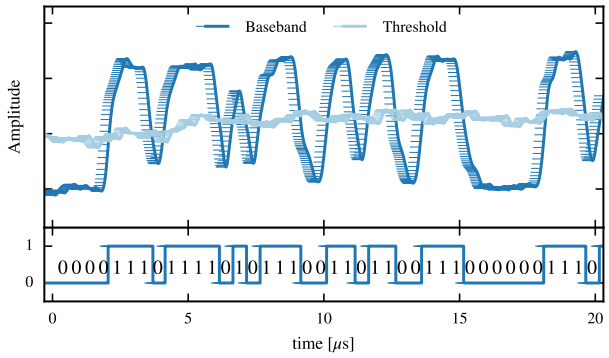

Figure 5: *Ultra-low power digitisation.* The upper panel shows the input signal of the comparator along with the corresponding threshold. The lower panel shows the digitised output signal.

digital demodulators. Third, analog phase demodulation is power hungry because it needs a LO synchronized with the remote carrier and obtaining this is energy demanding.

As an example, the budget for a full-blown state-of-the-art ultra-low-power receiver that consumes 3.8 mW [23, 25] has the following relative power consumption breakdown: The LNA (18%) and local oscillator (28%) are together responsible for half of the power consumption, the mixer consumes 9% while IF processing takes 13% and digital baseband processing consumes 32%.

We now examine these challenges in greater detail and present our corresponding solutions towards an ultra-low-power 802.15.4 receiver design as presented in Figure 2.

Challenge: Power-hungry RF front-end. High frequency RF components in conventional 802.15.4 receivers (Figure 3) are power hungry. An LNA boosts the high-frequency RF signal but is exposed to a wide range of signals impinging on the antenna. To avoid degrading the signal for later stages, the LNA needs high linearity and good noise performance, making the it a power-hungry component. Likewise, the RF LO is a power-hungry component due to the need to operate at high frequencies (ca. 2.4 GHz) while maintaining stability and low phase noise.

Solution. We replace the locally-generated oscillator by an externally-generated one in the form of an unmodulated carrier of frequency f_c. We employ a two-port diode mixer to down convert the signal to a much lower Intermediate Frequency $\Delta f = f - f_c$. Any undesired mixing products and harmonics are eliminated with the Band-Pass Filter (BPF). We forgo the power-hungry LNA sacrificing sensitivity, but we invest a small amount of power to bias the diode and regain sensitivity.

Challenge: Power-hungry digital demodulation. Implementing a digital demodulator requires digitizing the signal, but the required multi-bit high-speed ADCs have a power consumption in the order of milliwatts. Furthermore, the digitized signal is demodulated using numerical signal processing algorithms that make the digital demodulation block a power-hungry component.

Solution. We demodulate in the analog domain and digitize the baseband signal with a simple comparator and an energy-efficient thresholding circuit (Figure 2) similar to the ones applied in other works to receive ASK [19, 20, 22, 35]. This way, the DBP takes a single-bit input and is only in charge of recovering the data clock and despreading to recover the original data.

Challenge: Power-hungry phase demodulation. Analog phase demodulation can be power hungry because the incoming signal must be correlated with an LO that is synchronized with the remote carrier. Synchronizing the LO and the carrier requires a power-hungry feedback structure similar to a phase-locked loop [29]. Since the oscillator needs to have sufficient stability and low phase noise, it can also become power hungry.

Solution. We employ a passive slope detector (Figure 2) to demodulate the 802.15.4 signal efficiently. This is possible because the O-QPSK signal specified by the standard can be seen as a Minimum Shift Keying (MSK) signal. Equation 1 can be rearranged with the help of trigonometric identities:

$$S(t) = \cos\left[2\pi\left(f + b(t)\frac{1}{4T_c}\right)t + \Phi\right] \quad (2)$$

$b(t)$ depends only on the transmitted data and is -1 if $a_I(t) = a_Q(t)$ and 1 otherwise, Φ is a constant defined by the past history of the data.

The frequency of the signal in Equation 2 is $f + {}^{b(t)}/_{4T_c}$. Since $b(t)$ is 1 or -1, the 802.15.4 signal is modulated in frequency with a deviation ${}^{1}/_{4T_c}$. This is the minimum frequency deviation attainable while preserving orthogonality between the two frequency values [29], thus the name Minimum Shift Keying (MSK).

As a consequence, we can demodulate the 802.15.4 signal using a frequency detector, provided we correctly translate the frequency shifts to phase values. The MSK bit duration T_c is just enough for the signal's phase to change from one O-QPSK symbol to another in clockwise or counterclockwise direction, depending on the initial condition Φ. Although we do not know the initial phase, the DSSS chip sequences determine unique frequency shift patterns that are enough to recover the associated symbols. To that end, we adopt the approach by Notor et al. [24] and translate the spreading sequences

from the standard into the corresponding frequency-shift patterns. Our DBP (Figure 2) utilizes these translated sequences to despread the MSK signal.

4 IMPLEMENTATION

Our off-the-shelf prototype follows the architecture of Figure 2. We adopt the SMS7630 RF Schottky diode as a mixer. By adding a bias current we increase its mixing efficiency, hence improving the sensitivity of the receiver. A band-pass filter eliminates any undesired mixing products. We include an optional IF amplifier to further improve the sensitivity. Demodulation is implemented with a passive slope detector consisting of a filter to translate the frequency variations of the signal into amplitude variations (Figure 4). The amplitude variations are then extracted using a full-wave rectifier (Figure 4, right). The resulting signal is digitized by a comparator (MAX986) that compares the signal to a threshold defined by the signal's average (Figure 5). The DBP is implemented in an FPGA (Altera Cyclone IV) and is in charge of the DSSS despreading. The resulting data can be delivered from the DBP through any standard communication bus such as SPI or UART.

Choice of Δf. Our prototype operates with a signal-to-carrier frequency difference $\Delta f = 8$ MHz. This choice is motivated by a trade-off that exists as lower values of Δf facilitate getting an adequate roll-off in the slope detector. Higher values provide more room for filtering undesired mixing products with the BPF. To tune into an 802.15.4 channel, the receiver only needs an unmodulated carrier with a frequency 8 MHz below the channel's frequency.

Mixer. All mixers have a certain conversion loss that depends on several factors [26], including the strength of the input signals and the bias current. A Keysight's ADS [2] simulation indicates that, for our diode, a bias current of 0.75 mA produces the minimum conversion loss. Figure 6 shows the dependency of our mixer's conversion gain versus the signal strength of the carrier generator with applied bias and $\Delta f = 8$ MHz. The plot shows the variation of the strength of the intermediate frequency signal coming out of the mixer relative to the input signal strength for various values of the carrier power. The loss diminishes as the carrier signal gets stronger but it saturates as the diode switches entirely into conduction when the carrier approaches −12 dBm.

IF amplifier. An ultra-low-power amplifier compatible with our requirements does not exist as an off-the-shelf solution, but others have designed similar micropower amplifiers for other applications [5, 18, 32]. In our off-the-shelf prototype, we resort to an operational amplifier (ADA4940) to obtain 56 dB of IF voltage gain. The IF amplifier compensates for path loss, the mixer conversion loss and slope detector attenuation in order to provide an adequate signal to the comparator, and ultimately determines the communication range. Therefore we choose the gain based on the expected input signal strength for conventional transmitter output powers. We found that 56 dB offer a sufficient sensitivity while maintaining an attractive power consumption (Section 5). In Section 5.1 we discuss the design of an equivalent integrated ultra-low-power amplifier and its power consumption.

Digital Baseband Processor. The main functions of the DBP are to recover the data clock and to perform the DSSS despreading from a single-bit input with a relatively low bit rate of 2 Mbit/s as seen on the lower panel of Figure 5. Both of these functions can be implemented with simple low-power digital logic operating at relatively low clock frequencies. This ensures that an ultra-low-power IC implementation, similar to those used for transmission in other works [17, 20, 35], is feasible.

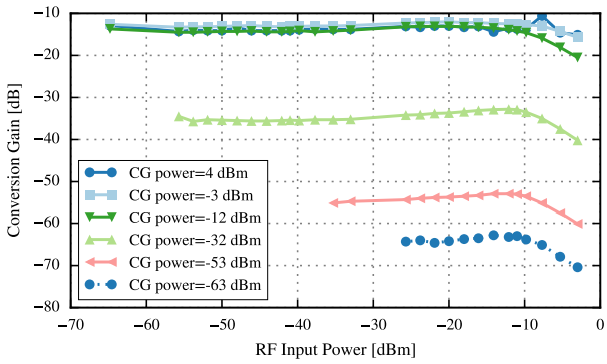

Figure 6: *Mixer conversion gain vs. input signal strength.* The bias current is 0.75 mA and $\Delta f = 8$ MHz. The conversion loss diminishes when the carrier generator signal (CG) strengthens but saturates around −12 dBm.

5 EVALUATION

In this section we evaluate our architecture. We perform experiments in a range of environments and conditions using two versions of the off-the-shelf prototype, one with IF voltage gain $G = 0$ dB and one with additional IF gain ($G = 56$ dB). We also evaluate the power consumption of an equivalent integrated design. Our main findings are:

- The sensitivity depends on the strength of the carrier. For the $G = 0$ dB case, the sensitivity is −8 dBm when the carrier generator is at least −7 dBm. For $G = 56$ dB, the value improves to −48 dBm for a −14 dBm carrier.
- The sensitivity for $G = 0$ dB is enough for a communication range in the order of tens of centimeters and requires relatively strong signals. When $G = 56$ dB the off-the-shelf prototype achieves a range of several meters while relaxing the signal strength requirements, making the receiver more practical at the expense of the extra power invested in the amplifier.
- If implemented in silicon, our design has a power consumption of 361 µW with an IF voltage gain $G = 60$ dB.

Table 1 shows a summary of the results of the evaluation and how they compare to current commercial receivers and the state of the art.

5.1 Power Consumption

The power consumption is the main concern for battery-free devices that operate with minuscule amounts of energy harvested from the environment. We begin the evaluation with the power consumption of our architecture, which is distributed among its several building blocks (Figure 2).

Table 1: *Comparison with existing 802.15.4 receivers.* Figures are for a −14 dBm carrier and $G = 56$ dB. Power consumption includes estimates of CMOS implementation. We improve the power consumption relative to commodity receivers by sacrificing performance.

RF Receiver	Sensitivity [dBm]	Consumption [mW]	Efficiency [nJ/bit]	$ACRR_1$ [dB]	$ACRR_2$ [dB]
CC2538	-88	40	160	44	52
AT86RF230	-101	27	108	34	52
EFR32MG1	-101	16	64	35	49
Liu et al. [23]	-100	3.8	15.2	-	-
Khan & Wentzloff [21]	-52	2.0	8.1	-	-
Our prototype	-48	0.36	1.4	20/14	24/22

$ACRR_1$/$ACRR_2$: Adjacent/Alternate Channel Rejection Ratio

Table 2: *Power consumption breakdown of the prototype.* The values for the IF amplifier and DBP are estimated upper bounds. The quiescent consumption is significantly lower.

Component	Mixer	IF amplifier	Comparator	DBP	**Total**
Consumption [μW]	66	75.2	190	29.8	361

The off-the-shelf components employed in the IF amplifier and the FPGA development board employed for the DBP have disproportionately high power consumptions that obscure the low power nature of our design. To evaluate the power consumption of our architecture, we follow the methodology of other recent works [17, 20, 30, 35] and design an IC version with a custom IF amplifier and DBP using a generic 45 nm bulk CMOS process. The power consumption figures reported for these components are based on the integrated designs.

Table 2 presents a breakdown of the power consumed by the active components. The rest of the blocks in our receiver are implemented with passive components such as resistors and capacitors and they do not draw additional supply power.

We invest power in biasing the diode mixer to improve the sensitivity. The power dissipated at the diode itself (bias current times the junction voltage) is 66 μW while maintaining the 0.75 mA bias current. One way to achieve such a bias current without dissipating additional power is with current reuse techniques commonly employed in low power integrated design [4].

The power consumption of the comparator depends on the frequency of transitions of the output. As a consequence, it consumes 55 μW while idle but needs 190 μW during data reception.

Integrated IF amplifier power estimation. In the off-the-shelf prototype, the IF amplifier is implemented with a general purpose operational amplifier. We argue that a satisfying ultra-low-power alternative can be implemented with existing CMOS technology. To that end, we have designed an integrated amplifier based on a generic 45 nm bulk CMOS process. With this design, we perform an analysis of the power consumption using Keysight's Advanced Design System (ADS) [2], an industry standard electronic design automation system.

The amplifier design consists of three common source cascode stages [28] that provide the bulk of the gain. Additionally, the last stage is a source follower in a push-pull configuration [28] to reduce the output impedance, making it adequate to drive the 1 kΩ load that our slope detector presents to the amplifier. Our analysis shows that this amplifier has a power consumption of 75.2 μW during reception while achieving a voltage gain of 60 dB. This power consumption figure is attainable because we are able to tailor the amplifier design to fit the needs of our design. Specifically, we take advantage of the fact that the required output power is in the order of microwatts.

Integrated DBP power estimation. To provide a realistic power estimation for the DBP we have translated the FPGA-based design into an equivalent silicon implementation based on a generic 45 nm CMOS process.

Our DBP operates on a single-bit input with a relatively low bit rate of 2 Mbit/s, and only needs to perform clock recovery and DSSS despreading at this low rate. We have evaluated the power consumption of the integrated design at the transistor level using Cadence Spectre, a fast and accurate circuit simulator widely used in the semiconductor industry [3]. Our CMOS implementation has an estimated power consumption of 29.8 μW while retaining functional compatibility with the FPGA-based prototype.

Overall consumption. The overall power consumption of our design is given by the sum of the power consumption of its building blocks. Table 1 shows the power consumption of our IC prototype would represent an improvement of two orders of magnitude when compared to current commodity 802.15.4 receivers and fivefold if compared to an IC implementation of a state-of-the-art receiver [21]. Specifically, our prototype has a power consumption of 361 μW and an efficiency of 1.4 nJ/bit.

5.2 Sensitivity

The sensitivity dictates the communication range and the required transmission power to achieve it. We adopt the definition of sensitivity dictated by the 802.15.4 standard [16]: The threshold signal strength where the Packet Reception Ratio (PRR) drops below 99% for a 20-byte PPDU.

Setup. The transmitter is a Zolertia Firefly node, a sensor platform based on the CC2538 SoC with an 802.15.4 transceiver. We employ a B200 Software Defined Radio (SDR) from Ettus Research for carrier generation, as it is more flexible and precise than Firefly nodes in performing power and frequency sweeps. Both devices are connected to the receiver using coaxial cables and an RF divider combiner to avoid the effects of multipath propagation. The carrier generator emits at $f_c = 2.472$ GHz while the Firefly transmits 20 byte-long packets on channel 26 ($f = 2.480$ GHz). As we will see (Figure 9), channel 26 is the least sensitive channel for our receiver. We repeat the experiment for various combinations of transmitter- and carrier-generator output power. The PRR is computed for each case. These experiments are performed with the off-the-shelf prototypes for IF gains $G = 0$ dB and $G = 56$ dB. Additionally, we measure the sensitivity across the different channels in the ISM band for $G = 56$ dB and a carrier generator power of −14 dBm. As we show next, this is the best sensitivity configuration we were able to achieve for $G = 56$ dB.

Results. Figure 7 depicts the result for $G = 0$ dB. The sensitivity remains practically constant at −8 dBm for all tested carrier powers.

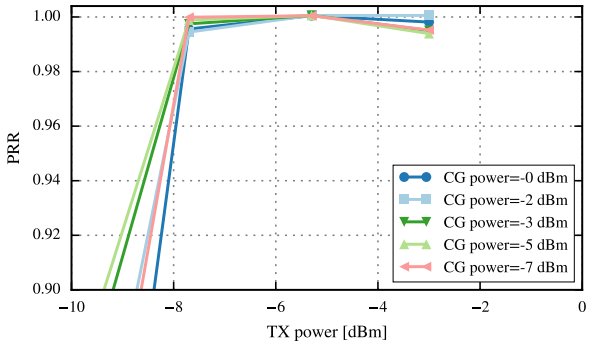

Figure 7: *PRR vs. transmitter and carrier generator power for* $G = 0$ dB. The sensitivity remains stable at −8 dBm.

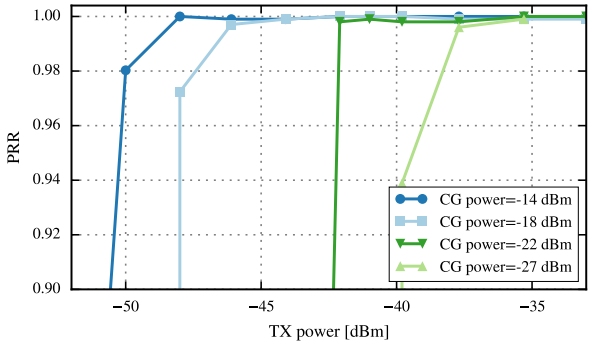

Figure 8: *PRR vs. transmitter and carrier generator power for* $G = 56$ dB. The sensitivity improves with carrier strength. For a −14 dBm carrier, the sensitivity is −48 dBm.

This highlights that the low power consumption of our receiver comes at the cost of performance.

With the addition of the $G = 56$ dB IF amplifier (Figure 8), the dependency of the sensitivity with the strength of the carrier is much more apparent. The sensitivity improves with the strength of the carrier generator. This trend should continue until the saturation point of the mixer as illustrated on Figure 6. For a −14 dBm carrier, the sensitivity is roughly −48 dBm, which enables communication ranges in the order of a few meters with transmitter and carrier powers around 0 dBm.

Figure 9 shows the sensitivity or our prototype across different 802.15.4 channels for a −14 dBm carrier and $G = 56$ dB. The receiver is about 6 dB more sensitive in channel 11 than in channel 26. This is likely due to small imperfections in the impedance matching network of the prototype that can be easily avoided with a better matching design.

5.3 Communication Range

The communication range determines the applicability of the receiver to real-life scenarios. We perform several experiments to illustrate the communication range achieved with our prototype.

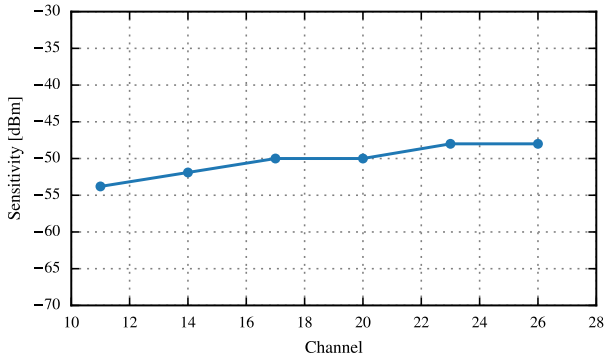

Figure 9: *Sensitivity over the 802.15.4 channels for* $G = 56$ dB *and a* −14 dBm *carrier.* The prototype has a small variation in sensitivity across the 2.4 GHz ISM band.

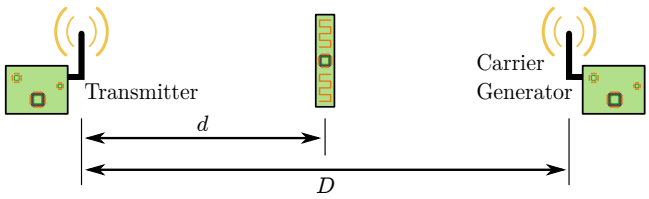

Figure 10: *Setup for range measurements.* The transmitter, receiver and carrier generator are located in a line. The distance from the transmitter to the receiver is d and to the carrier generator is D.

As in the previous experiments, we perform an evaluation for IF gains $G = 0$ dB and $G = 56$ dB.

Setup. The transmitter operates in channel 26, the least sensitive channel for our prototype. We place the transmitter, receiver and the SDR in a line as shown in Figure 10. The distance from the transmitter to the receiver is d and to the carrier generator is D. The SDR generates a carrier with frequency $f_c = 2.472$ GHz. All three devices use 3 dBi omnidirectional antennas, a typical choice in Wireless Sensor Networks (WSN) deployments. During the evaluation we change the distance d from 0 to D. The distance D is increased from a value where communication occurs at all values of d to a point where there is no communication almost at any point. In each configuration we measure the PRR. Unless otherwise stated, communication range experiments are performed in an anechoic chamber to keep interference and multipath propagation from impacting the measurement.

Results. Figure 11 shows the results for $G = 0$ dB. In this case the transmitter's output power is set to 20 dBm and the carrier generator transmits at 25 dBm. When the carrier generator is 60 cm from the transmitter, the prototype can be placed 30 cm from the transmitter and still achieve more than 99% PRR. For longer distances between the transmitter and carrier generator, the range is reduced.

With the addition of the IF amplifier ($G = 56$ dB), the communication range is extended significantly as shown in Figure 12. In this instance the transmitter's power is 3 dBm while the carrier generator emits a 0 dBm carrier. In this case, there are two zones of

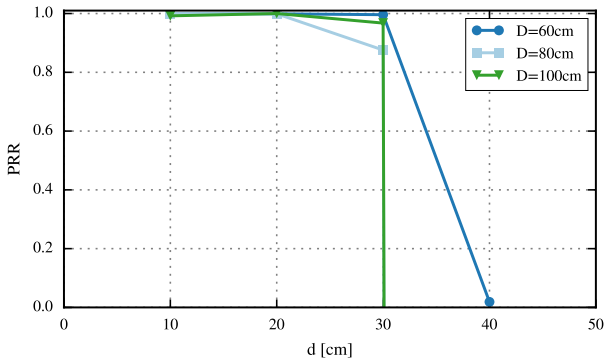

Figure 11: *Communication range for* $G = 0$ dB. PRR as a function of the distance between the transmitter and the receiver (d) for various values of the distance between the transmitter and the carrier generator (D).

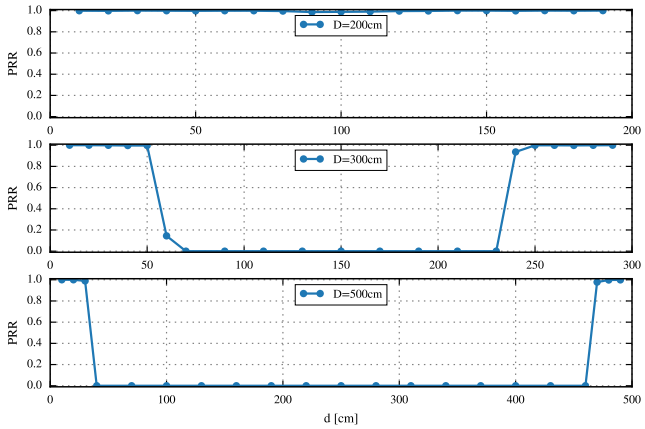

Figure 12: *Communication range for* $G = 56$ dB. Two zones of high packet reception rate exist: Closer to the transmitter and closer to the carrier generator. Those zones merge for smaller values of D.

flawless reception, when the receiver is placed next to either the carrier generator or the transmitter. The size of these zones grows as the carrier generator approaches the transmitter until both zones merge at a distance of roughly 200 cm. For a separation of 500 cm between the carrier generator and the transmitter both of the zones still have a radius of 30 cm. Note that these distance and power values are more than adequate to support short-range applications.

To further evaluate the impact of the IF amplifier on communication range, we perform one experiment with variable gain. The receiver is placed 30 cm from the carrier generator as this was the communication range obtained for the largest value of D in Figure 12. We measure the PRR at increasing values of D until communication breaks. We perform this experiment outdoors as the range exceeds the dimensions of the anechoic chamber. All other parameters remain the same as for the previous range experiments.

Figure 13 depicts the result of the experiment. As expected, the range increases steadily as the gain is increased. In these conditions

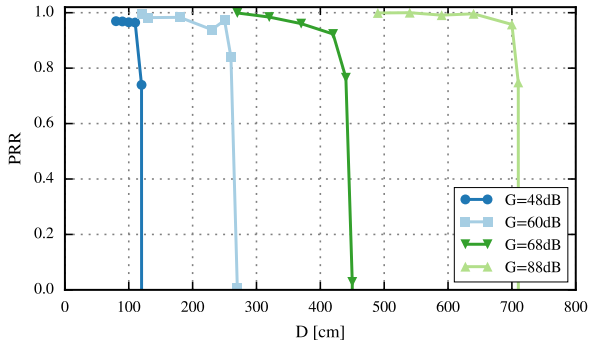

Figure 13: *Communication range vs. IF amplifier gain.* The communication range scales with the IF gain.

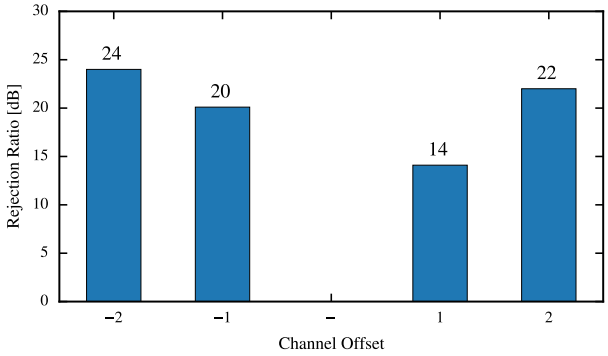

Figure 14: *Channel rejection ratio of the prototype.* The receiver features reasonable interference rejection. Values are for $G = 56$ dB and a carrier strength of -14 dBm.

we reach a range of almost 700 cm for the highest gain configuration achieved. We note that there is a range reduction relative to experiments in the anechoic chamber under otherwise similar conditions ($G = 60$ dB in Figure 13 vs. $D = 500$ cm in Figure 12). This is likely due to the higher noise levels of the outdoor environment.

5.4 Interference Resilience

Our receiver needs to simultaneously capture on the antenna the signal of interest and the remote carrier, but only employs the most basic interference mitigation mechanisms. Hence, we expect it to be more vulnerable to interference than commercial receivers. Consequently, we evaluate how the receiver is affected by the presence of an interfering 802.15.4 signal on the receiver's adjacent and alternate channels. We adopt the channel rejection ratio definition in the standard [16]: The ratio of interferer to signal strength where the PRR drops below 99% for a desired signal strength 3 dB above the sensitivity threshold.

We also show that due to the excellent out-of-band rejection of modern low-power transceivers, the presence of the unmodulated carrier is expected to have negligible impact on the regular transmissions of existing 802.15.4 networks.

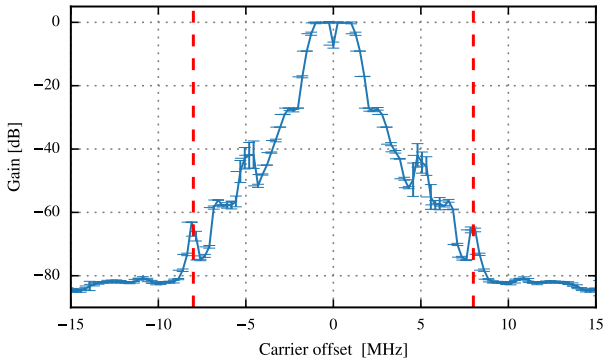

Figure 15: *CC2538 receiver filter attenuation versus channel frequency offset.* The red dashed lines represent the ±8 MHz marks where the attenuation is above 60 dB.

Setup. A Firefly node transmits in channel 18 at −47 dBm (that is 3 dB above the sensitivity for channel 18). The SDR generates a −14 dBm carrier, necessary to establish the appropriate sensitivity. Both devices are connected to the receiver using coaxial cables and an RF divider combiner. We measure the sensitivity for the alternate channels (±2 channel offsets) and the adjacent channels (±1 channel offsets).

Results. Figure 14 presents the result of this experiment. The interference rejection capabilities of the prototype are much weaker than those of commercial receivers in Table 1. However, a minimum channel rejection ratio of 14 dB means that interference on the adjacent channels needs to be at least 14 dB stronger than the desired signal to cause a significant drop in PRR.

Figure 15 shows the RSSI level reported by the CC2538 as it is presented with an unmodulated carrier of constant strength but varying frequency offset relative to the tuned channel. The attenuation is negligible inside the band of interest for 802.15.4 but it rapidly increases to more than 40 dB at the adjacent channel (5 MHz away). At an offset of 8 MHz, where our unmodulated carrier is located, the attenuation is larger than 60 dB. With this level of attenuation, the carrier should have no noticeable impact on the communications of nearby nodes. Furthermore, since the carrier only needs to be active for the duration of transmissions, a suitable coordination mechanism should help avoid collisions with regular transmissions from other nodes.

6 SENSOR TAG INTEGRATION

To illustrate how our receiver lowers the bar for the integration of battery-free devices into standard wireless networks, we couple our prototype with a backscatter transmitter. This transmitter synthesizes 802.15.4 signals in the presence of an unmodulated carrier while consuming tens of microwatts. We leverage the radio test mode, accessible in many transceivers to aid in regulatory licensing, as the means to generate an unmodulated carrier required by both transmitter and receiver [27, 33].

6.1 Tag Interrogation with TSCH

Time-Slotted Channel Hopping (TSCH) is one of several MAC protocols defined in the IEEE 802.15.4 standard [16]. In a TSCH network, nodes form a mesh that is synchronized by the PAN coordinator.

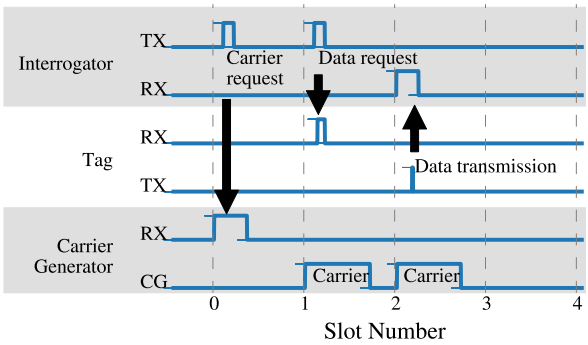

Figure 16: *Our battery-free passive sensor integrates with a TSCH network.* The interrogator node coordinates carrier generation with a neighbor. During the next two timeslots the generated carrier is used to transmit to and from the battery-free device. The slot duration is 10 ms.

Time is divided into slots that last 10 ms by default, enough time for a node to receive a frame and transmit an acknowledgement. A series of timeslots form a slotframe that cyclically repeats in time. Each node may have its own schedule that dictates what to do during each time slot, whether to receive, transmit or remain idle. The schedule also indicates the channel on which to receive or transmit during any given timeslot.

The time-slot structure of TSCH makes is particularly appropriate to schedule the carrier generation. It is easy to envision future scheduling mechanisms that try to increase efficiency by maximizing carrier reuse for both transmission and reception.

In this scenario we demonstrate how Passive Sensor Tags (Figure 1) seamlessly integrate with nodes running TSCH. Passive Sensor Tags are battery-free devices that extend the sensing capabilities of current wireless sensor networks [27]. To add a new sensor or replace a broken one, one simply places a sensor tag containing the new sensor next to one of the existing active nodes.

We have extended the TSCH implementation [10] in the Contiki operating system by adding a new type of timeslot dedicated to carrier generation. With this extension the nodes remain compatible with TSCH and follow their schedules as usual. When a carrier generation timeslot is active, the node generating the carrier first sets its radio to transmit at a frequency that is $\Delta f = 8$ MHz lower than the frequency normally associated with the timeslot according to the TSCH schedule. Then the node activates its radio test mode to transmit the carrier, which lasts for the duration of the timeslot. With this alteration, our prototype can integrate in the TSCH network.

Figure 16 depicts a logic analyzer trace that shows how the process shown in Figure 1 unravels. During timeslot 0, the interrogating node sends a carrier request message to the carrier generator to activate its carrier slots. During the next two timeslots, the carrier generator emits an unmodulated carrier at the appropriate frequency. During timeslot 1, the interrogating node sends its data

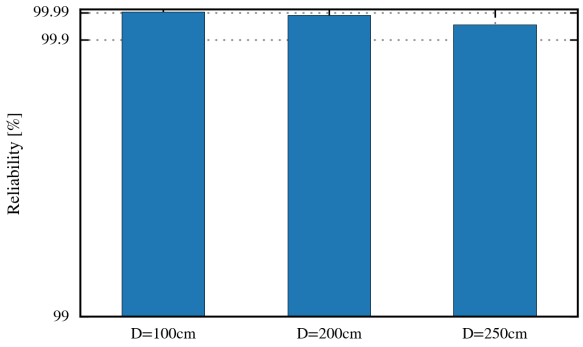

Figure 17: *TSCH long-term reliability for d = 15 cm.* The receiver can be highly reliable in real-life conditions. We performed more 500 000 interrogation cycles with 3 dBm carrier and transmitter output powers.

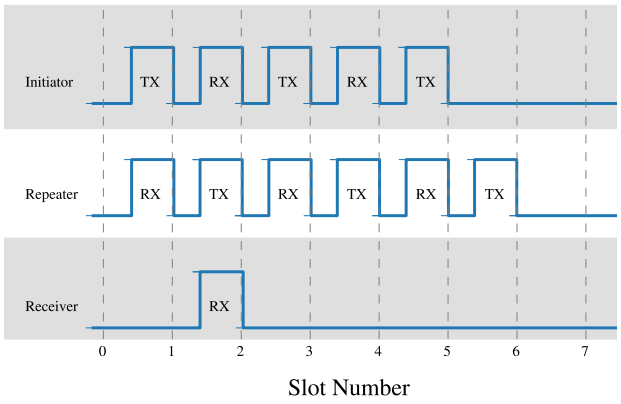

Figure 18: *Our battery-free sensor integrates with a Glossy network.* The tag only needs to receive one of the N transmissions and does not participate in retransmissions. The slot duration is 1 ms. The carrier is generated continuously but not shown.

request message to the sensor tag. During timeslot 2, the tag leverages the carrier to perform its data transmission containing the sensor reading. This cycle may be repeated during the next slotframe. If we want to dispense with the carrier and data requests in Slots 0 and 1, Slot 2 can be executed on a fixed schedule. We leave specific slot assignment strategies for future work.

6.2 Long-Term Reliability

One of the reasons that makes battery-free devices attractive is that they can operate unattended for long periods. In such a scenario, the long-term reliability of the device, and in particular of its communication functions, become critical. We perform an experiment that illustrates the overall reliability of our receiver over a long period of operation.

We set our sensor tag prototype to operate alongside the TSCH devices in our lab environment while regular activities take place. The interrogator node is located 15 cm from the receiver while it periodically performs the interrogation cycle described in Section 6.1. We log the number of successful and missed interrogation cycles for more than 500 000 cycles spanning over 20 hours. We perform the same experiment for various distances D between the transmitter and carrier generator. Both nodes transmit at 3 dBm.

The result of this experiment (Figure 17) shows a reliability well above 99% on the conditions tested. For an instance of this experiment with D = 100 cm we obtain a reliability above 99.99%. In this instance 515 432 request cycles were performed, out of which the receiver only missed 37. The reliability worsens slightly as the distance to the carrier generator increases. At D = 250 cm it is still above 99.9%. In this experiment we do not employ any retransmission mechanisms. Our results show that the receiver can be highly reliable in real-life operating conditions.

6.3 Glossy Integration

Glossy is a network flooding protocol that exploits concurrent transmissions to achieve highly energy-efficient and reliable communication [14]. Glossy lends itself, for instance, to performing over-the-air firmware upgrades to multiple sensor tags installed throughout a wireless sensor network.

We test this scenario by transferring data to our receiver using an unmodified implementation of Glossy compatible with the Zolertia Firefly [15]. Figure 18 depicts how this exchange happens. In this case, Glossy is configured to perform three transmissions in each Glossy phase (N = 3). The battery-free device does not participate in the retransmission scheme given that the backscattered signal is too weak to have a significant impact faced with the stronger signal from the active transmitters. The device can still operate as initiator without problems. The carrier wave can be provided by an external device as is done in other works [20, 30, 33] or by one of the members of the Glossy network using the carrier test mode mentioned earlier. In the latter case, the carrier can be supplied continuously during the active Glossy period by designated nodes or nodes can switch to generating a carrier instead of retransmitting once they have received the packet. In our setup the carrier is supplied continuously by an SDR.

Our receiver operates with considerably less sensitivity than sensor nodes equipped with a full-blown receiver. Therefore, it does not benefit significantly from the concurrent transmissions mechanism in Glossy. In our scenario the network still benefits from the reliability, and the efficient data dissemination of Glossy by propagating the firmware upgrade with minimal overall energy cost to the network.

For other scenarios the sensor tag transmitter can operate as the initiator in the Glossy network. This opens the possibility of integrating our sensor tags into networks running other Glossy-based protocols such as the Low-power Wireless Bus [13].

7 DISCUSSION

Need for an external carrier. A fundamental characteristic of our receiver architecture is the need for an external carrier generator. This is a shared trait with backscatter transmitters, which

makes them an ideal combination. Previous backscatter communication works feature numerous alternatives to provide the carrier [17, 27, 33], with various levels of trade-offs. In this work, we demonstrate one way in which standard 802.15.4 nodes can exploit their radio test mode to provide a carrier, while requiring only software modifications but there are many other possibilities. With many different approaches to carrier generation, we believe that the need for the carrier should not pose a major obstacle in most applications. Instead, the application will probably dictate the choice of carrier generator depending on a combination of design factors.

Communication range. Our evaluation shows that we achieve sufficient communication range for integrating within conventional sensor networks. Our results are significant for short-range sensor network applications with high node density, e.g. automotive applications [9] and structural health monitoring [6].

When we use an IF amplifier, our results show two zones of error-free reception. The first zone surrounds the transmitter. As in conventional radio receivers, the reception probability in this zone decreases as the receiver moves away from the transmitter. The second zone appears around the carrier generator. In this case, the reception probability increases as the receiver moves closer to the carrier generator. The cause of this behaviour is the dependency of the conversion loss of the diode mixer with the signal strength of both input signals (Figure 6). This phenomenon has no parallel in conventional radio receivers. However, it closely resembles a similar phenomenon that appears with backscatter transmitters [20, 27].

Other protocols. We have shown that our tags integrate with TSCH and Glossy networks. Another 802.15.4-based protocol is Thread [1]. Thread requires that all routers are mains-powered. Thread routers could hence prove ideal to provide the required carriers for both reception and backscatter transmission to integrate battery-free devices.

Our receiver architecture is also compatible with the reception of other wireless protocols. Specifically, it can be made to receive BLE packets by simply adding a compatible baseband processor. Similarly, our receiver could be made compatible with the Gaussian Minimum Shift Keying modulation employed in GSM networks as it has similar properties as O-QPSK. On this light, it is not hard to envision the battery-free reception of SMS messages for a battery-free cellphone [31].

Applications. Battery-free sensors are easier to maintain than their battery-powered counterparts since there is no need to exchange batteries, which is cumbersome and expensive, in particular in countries where labor cost is high. Our work enables the integration of battery-free sensors into networks where some nodes are battery-powered or even mains-powered (as, for example, mandated by Thread) and hence can support a larger number of battery-free devices. This is especially useful in denser deployments such as in home and building automation applications. Battery-free sensors are also very useful when sensors need to be placed in locations where they cannot be reached easily to exchange batteries once deployed. Examples include sensors in walls or under the floor, behind rotating equipment, in toys or sensors implanted in the body. For example, one of the Swedish insurance companies has a yearly cost of more than 120 Million Dollar for water leakage in kitchens and bathrooms which could be reduced drastically with battery-free humidity sensors under the floors.

8 CONCLUSIONS

We have introduced the architecture of an 802.15.4 receiver that consumes only 361 µW, making it compatible with novel battery-free applications. The receiver, when paired with a backscatter 802.15.4 transmitter enables micropower devices that, for the first time, directly interoperate with unmodified 802.15.4 transceivers. As we have shown, this significantly lowers the bar for applications where battery-free devices interoperate with standard wireless sensor networks.

ACKNOWLEDGEMENTS

We thank our shepherd Brad Campbell for his constructive feedback towards the final version of this paper. This work has been partly funded by the Internet Foundation in Sweden through Internetfonden, by the Swedish Knowledge Foundation (Grant 20140319) and the Swedish Research Council (Grant 2017-045989).

REFERENCES

[1] 2017. Thread. (2017). https://threadgroup.org/
[2] 2018. Advanced Design System (ADS). (2018). https://www.keysight.com/en/pc-1297113/advanced-design-system-ads
[3] 2018. Cadence Spectre. (2018). https://www.cadence.com/content/cadence-www/global/en_US/home/tools/custom-ic-analog-rf-design/circuit-simulation/spectre-circuit-simulator.html
[4] U. Alvarado, G. Bistué, and I. Adín. 2011. *Low Power RF Circuit Design in Standard CMOS Technology.* Springer Science & Business Media.
[5] I. U. Baimei, L., C. Wang, M. A. Minglin, and G. U. O. Shengqiang. 2009. An ultra-low-voltage and ultra-low-power 2.4 GHz LNA design. *Radioengineering* 18, 4 (2009), 527.
[6] S. Banerji, A. Bagchi, and S. Khazaeli. 2016. STR-991: Energy Harvesting Methods for structural health monitring using wireless sensors: a review. *Canadian Society for Civil Engineering* (June 2016).
[7] Naveed Anwar Bhatti, Muhammad Hamad Alizai, Affan A. Syed, and Luca Mottola. 2016. Energy Harvesting and Wireless Transfer in Sensor Network Applications: Concepts and Experiences. *ACM Trans. Sen. Netw.* 12, 3, Article 24 (Aug. 2016), 40 pages. https://doi.org/10.1145/2915918
[8] C. Bryant and H. Sjöland. 2014. A 0.55 mW SAW-Less Receiver Front-End for Bluetooth Low Energy Applications. *IEEE Journal on Emerging and Selected Topics in Circuits and Systems* 4, 3 (Sept. 2014), 262–272.
[9] J. Carmo et al. 2010. A 2.4-GHz CMOS Short-Range Wireless-Sensor-Network Interface for Automotive Applications. *IEEE Trans. Ind. Electron.* 57, 5 (May 2010), 1764–1771.
[10] Simon Duquennoy, Atis Elsts, B. A. Nahas, and George Oikonomou. 2017. TSCH and 6TiSCH for Contiki: Challenges, Design and Evaluation. *IEEE DCOSS* (2017).
[11] J. F. Ensworth, A. T. Hoang, and M. S. Reynolds. 2017. A low power 2.4 GHz superheterodyne receiver architecture with external LO for wirelessly powered backscatter tags and sensors. In *2017 IEEE International Conference on RFID (RFID)*. 149–154. https://doi.org/10.1109/RFID.2017.7945601
[12] J. F. Ensworth and M. S. Reynolds. 2015. Every smart phone is a backscatter reader: Modulated backscatter compatibility with Bluetooth 4.0 Low Energy (BLE) devices. In *IEEE RFID 2015*.
[13] Federico Ferrari, Marco Zimmerling, Luca Mottola, and Lothar Thiele. 2012. Low-power Wireless Bus. In *SenSys '12*. ACM, 1–14.
[14] Federico Ferrari, Marco Zimmerling, Lothar Thiele, and Olga Saukh. 2011. Efficient network flooding and time synchronization with Glossy. In *IPSN'11*. 73–84.
[15] Kasun Hewage, Shahid Raza, and Thiemo Voigt. 2017. Protecting Glossy-based Wireless Networks from Packet Injection Attacks. In *IEEE MASS 2017*.
[16] IEEE. 2015. *IEEE Standard for Low-Rate Wireless Networks.* 709 pages.
[17] Vikram Iyer, Vamsi Talla, Bryce Kellogg, Shyamnath Gollakota, and Joshua Smith. 2016. Inter-Technology Backscatter: Towards Internet Connectivity for Implanted Devices. In *Proceedings of the 2016 ACM SIGCOMM Conference (SIGCOMM '16)*. ACM, New York, NY, USA, 356–369. https://doi.org/10.1145/2934872.2934894
[18] Gh. R. Karimi and S. Babaei Sedaghat. 2012. Ultra low voltage, ultra low power low noise amplifier for 2GHz applications. *AEU - International Journal of Electronics and Communications* 66, 1 (Jan. 2012), 18–22.

[19] Bryce Kellogg, Aaron Parks, Shyamnath Gollakota, Joshua R. Smith, and David Wetherall. 2014. Wi-fi Backscatter: Internet Connectivity for RF-powered Devices. In *Proceedings of the 2014 ACM Conference on SIGCOMM (SIGCOMM '14)*. ACM, New York, NY, USA, 607–618. https://doi.org/10.1145/2619239.2626319

[20] Bryce Kellogg, Vamsi Talla, Shyamnath Gollakota, and Joshua R. Smith. 2016. Passive Wi-Fi: Bringing Low Power to Wi-Fi Transmissions *(NSDI '16)*. 151–164.

[21] O. U. Khan and D. D. Wentzloff. 2015. 8.1 nJ/b 2.4 GHz Short-Range Communication Receiver in 65 nm CMOS. *IEEE Transactions on Circuits and Systems I: Regular Papers* 62, 7 (July 2015), 1854–1862.

[22] Vincent Liu, Aaron Parks, Vamsi Talla, Shyamnath Gollakota, David Wetherall, and Joshua R. Smith. 2013. Ambient Backscatter: Wireless Communication out of Thin Air. In *Proceedings of the ACM SIGCOMM 2013 Conference on SIGCOMM (SIGCOMM '13)*. ACM, New York, NY, USA, 39–50. https://doi.org/10.1145/2486001.2486015

[23] Y. H. Liu et al. 2013. A 1.9nJ/b 2.4GHz multistandard (Bluetooth Low Energy/Zigbee/IEEE802.15.6) transceiver for personal/body-area networks. In *2013 IEEE International Solid-State Circuits Conference Digest of Technical Papers*. 446–447.

[24] J. Notor et al. 2003. CMOS RFIC architectures for IEEE 802.15. 4 networks. *Cadence Design Systems, Inc* 41 (2003).

[25] K. Philips. 2014. Ultra low power short range radios: Covering the last mile of the IoT. In *ESSCIRC 2014* (2014). IEEE, 51–58.

[26] D. Pozar. 2011. *Microwave Engineering* (4th ed.). Wiley.

[27] Carlos Pérez-Penichet, Frederik Hermans, Ambuj Varshney, and Thiemo Voigt. 2016. Augmenting IoT Networks with Backscatter-enabled Passive Sensor Tags. In *Proceedings of the 3rd Workshop on Hot Topics in Wireless (HotWireless '16)*. ACM, New York, NY, USA, 23–27. https://doi.org/10.1145/2980115.2980132

[28] A. S. Sedra and K. C. Smith. 2014. *Microelectronic Circuits* (7th ed.). Oxford University Press.

[29] Simon Haykin. 2009. *Communication Systems* (5th ed.). Wiley, Hoboken, NJ.

[30] Vamsi Talla, Mehrdad Hessar, Bryce Kellogg, Ali Najafi, Joshua R. Smith, and Shyamnath Gollakota. 2017. LoRa Backscatter: Enabling The Vision of Ubiquitous Connectivity. *Proc. ACM Interact. Mob. Wearable Ubiquitous Technol.* 1, 3, 105:1–105:24. https://doi.org/10.1145/3130970

[31] Vamsi Talla, Bryce Kellogg, Shyamnath Gollakota, and Joshua R. Smith. 2017. Battery-Free Cellphone. *Proc. ACM Interact. Mob. Wearable Ubiquitous Technol.* 1, 2, 25:1–25:20. https://doi.org/10.1145/3090090

[32] M. R. Valero et al. 2015. A high-performance 1.2V–99uW rail-to-rail CMOS class AB amplifier. *Microelectronics Journal* 46, 1 (2015), 96–102.

[33] Ambuj Varshney, Oliver Harms, Carlos-Perez Penichet, Christian Rohner, Frederik Hermans, and Thiemo Voigt. 2017. LoRea: A Backscatter architecture that achieves a long communication range. In *ACM SenSys 2017*. ACM Digital Library.

[34] Anran Wang, Vikram Iyer, Vamsi Talla, Joshua R. Smith, and Shyamnath Gollakota. 2017. FM Backscatter: Enabling Connected Cities and Smart Fabrics.. In *NSDI*. 243–258.

[35] Pengyu Zhang, Dinesh Bharadia, Kiran Joshi, and Sachin Katti. 2016. HitchHike: Practical Backscatter Using Commodity WiFi. In *Proceedings of the 14th ACM Conference on Embedded Network Sensor Systems CD-ROM (SenSys '16)*. ACM, New York, NY, USA, 259–271. https://doi.org/10.1145/2994551.2994565

[36] Pengyu Zhang, Pan Hu, Vijay Pasikanti, and Deepak Ganesan. 2014. EkhoNet: High Speed Ultra Low-power Backscatter for Next Generation Sensors. In *Proceedings of the 20th Annual International Conference on Mobile Computing and Networking (MobiCom '14)*. ACM, New York, NY, USA, 557–568. https://doi.org/10.1145/2639108.2639138

[37] Pengyu Zhang, Mohammad Rostami, Pan Hu, and Deepak Ganesan. 2016. Enabling Practical Backscatter Communication for On-body Sensors. In *Proceedings of the 2016 Conference on ACM SIGCOMM 2016 Conference (SIGCOMM '16)*. ACM, New York, NY, USA, 370–383. https://doi.org/10.1145/2934872.2934901